Natural convection in a triangular enclosure induced by solar radiation

Yadan Mao, Chengwang Lei and John Patterson

School of Engineering, James Cook University, Townsville, QLD, 4811, Australia

Abstract

Natural convection in a triangular enclosure induced by solar radiation is simulated and analyzed. The numerical simulation reveals three possible distinct flow regimes in the enclosure. It also reveals the variations of the dominant heat transfer mode and the flow status with the horizontal position along the wedge. The whole domain can be divided horizontally into several regions according to the dominant mode of heat transfer. For small Rayleigh numbers, heat transfer over the entire domain is dominated by conduction. For medium Rayleigh numbers, there are two distinct regions. Heat transfer in the near shore region is dominated by conduction. As the distance from the shore increases, stable convection becomes the dominant mode. The region dominated by stable convection expands with increasing Rayleigh number. For high Rayleigh numbers, the whole region can be divided into three distinct regions where the dominant mode of heat transfer changes from conduction to stable convection and then to unstable convection as the distance from the shore increases. The region of flow instability also expands with increasing Rayleigh number.

Introduction

Natural convection in littoral regions plays an important role in the transport of nutrients and pollutants across reservoirs, lakes and other geophysical water bodies. A triangular geometry has been assumed to represent the bathymetry variation in the littoral regions. Since an approximately equal flux of heating or cooling at the surface is distributed over different depths of water, the water will become either warmer or cooler than its horizontally neighbouring regions. The horizontal temperature gradient then results in a horizontal density gradient, which is an important driving force of convective flows in natural water bodies.

Field observations [1,7] have provided evidence demonstrating the significance of this horizontal buoyancy driven flow induced by differential water depths. The functioning of the thermal siphon substantially reduces the time required to replace the water in sidearms of reservoirs.

During the daytime, the water body absorbs solar radiation in an exponentially decaying manner with the water depth according to Beers' law. Typically, in natural water bodies, most radiation is absorbed between the surface and a depth of about 1-2 meters, resulting in a shallow surface layer with water much warmer than the underlying water. Near the shore where the depth of the water body is less than the penetration depth, two models have been adopted for the absorption of solar radiation by the water. One model is that all of the radiation was absorbed and uniformly distributed over the local water depth. This model was proposed by [3] in an analysis of diurnal cycles, which leads to an increasing rate of heating with the decreasing water depth. The other model [4] approaches the issue in a more physically realistic way. It took into account the exponential decaying absorption of solar radiation described by Beer's law, and any residual radiation reaching the bottom was assumed to be absorbed by the bottom, and the absorbed energy re-emitted as a

bottom heat flux, which was a potential source for Rayleigh-Benard instability. This model was also adopted in [6], in which a scaling analysis classified the overall flow at different Rayleigh numbers into three flow regimes, namely, a conductive, a transitional and a convective regime. The scaling in [6] provides an overall description of the flow status over the whole domain at different parametric settings. However, the scaling did not capture the variation of the flow status and heat transfer with the horizontal position, which may be resulted from the changing water depth.

The numerical simulation presented in this paper focuses on the variation of the dominant mode of heat transfer and the flow status with the horizontal position. Identifying the different flow regions will provide important insights into the exchange flows occurring at different sections of the sidearm since the transportation processes vary with the horizontal position.
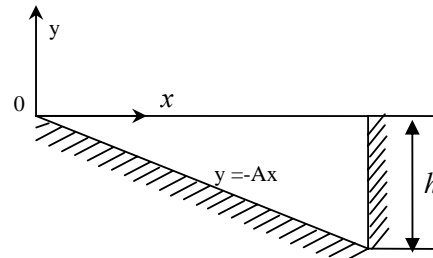
Model Formulation

Figure 1 Geometry of the flow domain

The daytime circulation in the sidearm is modelled with a wedge with a bottom slope of A and a depth of h (Fig 1). With Boussinesq assumption, the Navier-Stokes and energy equations governing the flow and temperature evolution within the wedge can be written as:

$$\frac{\partial u}{\partial x} + \frac{\partial v}{\partial y} = 0 \tag{1}$$

$$\frac{\partial u}{\partial t} + u\frac{\partial u}{\partial x} + v\frac{\partial u}{\partial y} = -\frac{1}{\rho_0}\frac{\partial p}{\partial x} + v\nabla^2 u \tag{2}$$

$$\frac{\partial v}{\partial t} + u\frac{\partial v}{\partial x} + v\frac{\partial v}{\partial y} = -\frac{1}{\rho_0}\frac{\partial p}{\partial y} + v\nabla^2 v + g\beta(T - T_0) \tag{3}$$

$$\frac{\partial T}{\partial t} + u\frac{\partial T}{\partial x} + v\frac{\partial T}{\partial y} = k\nabla^2 T + S(x,y,t) \tag{4}$$

where u and v are the velocity components in the horizontal and vertical directions, x and y are the horizontal and vertical coordinates originating from the tip; T is the fluid temperature; p is the pressure. The density, kinematic viscosity, thermal diffusivity and thermal expansion of the fluid at the reference temperature T_0 are represented by ρ_0, v, k and β respectively. $S(x,y,t)$ represents the internal heating source due to absorption of solar radiation. The radiation intensity at a

particular wavelength decrease with the water depth according to Beer's law:

$$I = I_0 e^{\eta y} \qquad y \le 0 \qquad (5)$$

where I_0 is the radiation intensity at the water surface, η is the attenuation coefficient of water which is a function of the wavelength of the incident radiation and the turbidity of water [5]. The attenuation coefficient is often assumed to be constant in applications to simply the problem, and this assumption is also adopted here. Therefore, the source term in equation (4) is given by:

$$S = H_0 \eta e^{\eta y} \qquad -Ax \le y \le 0 \qquad (6)$$

where $H_0 = I_0 / (\rho_0 C_p)$, and C_p is the specific heat of water at the reference temperature.

The internal source term in equation (6) generates a stable stratification in the water column. For the shallow region, there will be a considerable amount of radiation reaching the bottom. It is assumed that all the radiation reaching the bottom is absorbed by the bottom, and the absorbed energy is reemitted in the form of a boundary heat flux. The source that generates fluid motion comes from the bottom heat flux, which also creates a potentially unstable temperature gradient. The thermal boundary condition of the bottom surface can thus be defined as:

$$\frac{\partial T}{\partial \hat{n}} = -\frac{1}{k} H_0 e^{-A\eta x} \qquad (7)$$

where $\hat{n}$ is the direction normal to the sloping bottom.

In the following numerical simulations, rigid non-slip velocity boundary conditions ($u = v = 0$) are assumed for the water surface, the end wall, and the bottom. An adiabatic temperature condition is assumed for the water surface and the end wall. Apart from creating an additional viscous layer near the surface, the non-slip boundary condition is not expected to affect the overall flow feature.

There is no flow or heat transfer in the enclosure before the radiation starts. As soon as the radiation is initiated, the water temperature starts to increase due to the absorption of the radiation entering the water body. Due to the effect of the bottom heat flux specified in equation (7), a thermal boundary layer develops along the bottom slope. The thickness δ_T of the thermal boundary layer can be derived from a balance between the unsteady and diffusion terms in the energy equation:

$$\delta_T \sim (kt)^{1/2} \qquad (8)$$

Hence the temperature scale in the bottom thermal boundary layer is given by

$$T_b \sim \frac{1}{k} H_0 \delta_T e^{-A\eta x} \sim k^{-1/2} t^{1/2} H_0 e^{-A\eta x} \qquad (9)$$
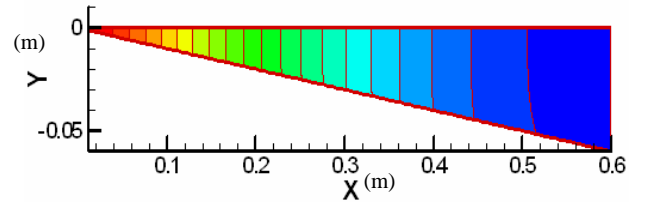
Numerical Results
The governing equations (1)-(4) along with the specified boundary and initial conditions are solved numerically using a finite volume method. The SIMPLE scheme is adopted for pressure-velocity coupling; and a third-order discretization scheme is applied for spatial derivatives. A second-order implicit scheme is applied for time discretization in calculating the transient flow. The geometric and flow parameters used in the simulations are: $A = 0.1$, $h = 0.06$ m, $\eta = 2$, and thus the problem falls into the shallow-water case for which $h < 1/\eta$. Prandlt number Pr is defined as $\text{Pr} = v/k$, and $\text{Pr} = 7$ is assumed for the water. The intensity of natural convection inside

the wedge depends upon the Grashof number (Gr) or the Rayleigh number (Ra), which are defined as:
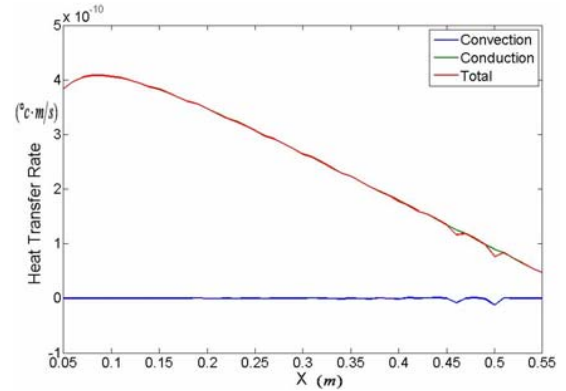
$$Gr = \frac{g\beta H_0 h^4}{v^2 k} \qquad (10)$$

$$Ra = \text{Pr} \cdot Gr \qquad (11)$$

In order to simulate the flow under different radiation intensities, the Grashof number in the simulations varies over a wide range from 10 to 2×10^6. It will be shown later that this range of the Grashof numbers covers all the possible flow regimes for the specified problem.

(a)   Temperature contour at the steady state for Gr=10

(b) The horizontal heat transfer rate at the steady state averaged over the local water depth at different horizontal locations for Gr=10

Figure 2 Temperature contours and horizontal heat transfer rate at a typical low Grashof number at which conduction dominates the whole flow domain

Figure 2 shows the typical feature of heat transfer for small Rayleigh numbers. At the steady state, the temperature contours are vertical over virtually the whole domain (Figure 2 (a)), which indicates that conduction dominates heat transfer. The horizontal heat transfer rate is averaged over the local depth and is defined as:

$$H(x) = \frac{1}{Ax} \int_{-Ax}^{0} (uT - k\frac{\partial T}{\partial x})dy \qquad (12)$$

where T is the difference between the local temperature and the average temperature over the whole domain. The term uT , $-k\frac{\partial T}{\partial x}$ specify the horizontal heat transfer generated by convection and conduction respectively. Figure 2 (b) suggests that conduction is the dominant means of heat transfer over the whole domain at this Grashof number. The bottom thermal boundary layer starts to grow due to heat transfer from the bottom boundary to the interior as soon as the radiation is initiated. Since the Grashof number is small, convection is weak, and is insufficient to balance conduction. The amount of heat conducted into the boundary layer will be always larger than that convected away. Therefore, the thermal boundary layer keeps

growing until it encompasses the entire flow domain. In this case, no distinct thermal boundary layer can be identified at the steady state.
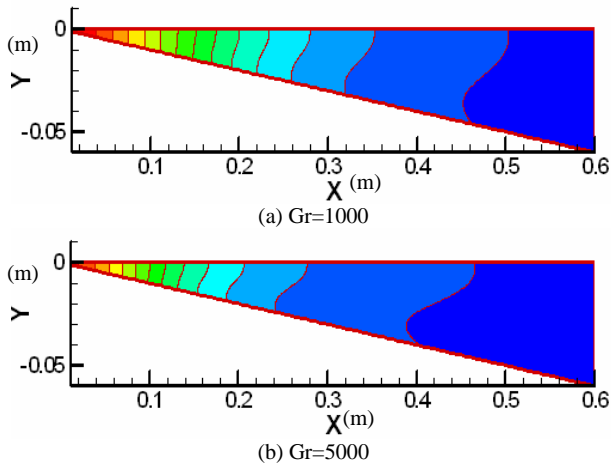

(a) Gr=1000

(b) Gr=5000

Figure 3 Temperature contours at the steady state for Grashof numbers in the medium range in which conduction dominates in the tip region and convection dominates in deeper regions.

As the Rayleigh number increases, the scenario becomes different. The bottom thermal boundary layer starts to grow by conduction after the radiation is initiated. As time goes on, convection is getting stronger and becomes increasingly important. At a certain point of time, heat conducted into the thermal boundary layer is balanced by that convected away. The thermal boundary layer then ceases to grow, and the flow becomes steady. If at this time, the bottom thermal boundary layer has not grown to the full local water depth, then a distinct thermal boundary layer is present. Figure 3 shows the temperature contours at the steady state at two Grashof numbers Gr = 1000 and 5000. It is seen in figure 3 that, near the tip region, the isotherms are vertical, implying the dominance of conductive heat transfer in that region. Further away from the tip, the isotherms above the bottom tilt upwards, and the degree of tilting increases with the distance from the tip. This temperature structure suggests that convection becomes more important as the distance from the tip increases. The curvature of the temperature contours also suggests the existence of a distinct bottom thermal boundary layer.

For regions near the tip, since the local water depth is small, the thermal boundary layer reaches the top surface before convection becomes strong enough to balance conduction. Therefore, the thermal boundary layer is indistinct near the tip. As the distance from the tip increases, it takes longer for the thermal boundary layer to grow to the top surface. Before the thermal boundary layer reach the local top surface, convection become sufficiently strong to balance conduction at a critical time t_c, and the thermal boundary layer ceases to grow and remains distinct. A comparison of Figures 3(a) and (b) indicates that, as the Grashof number increases, the region dominated by convection increases and expands toward the tip end. The curvature of isotherms also increases with the Grashof number, signifying an increasing flow velocity.

Figure 4 shows the horizontal heat transfer rate (averaged over the local depth) by conduction and convection respectively. The trend revealed in the temperature contours in Figure 3 is further verified in Figure 4. In this figure, the point at which conduction heat transfer is equal to convection heat transfer identifies the critical horizontal position $x = a$, which separates the regions with and without a distinct thermal boundary layer. This horizontal position also marks the dividing point where the dominated mode of horizontal heat transfer switches between conduction and convection. As the Grashof increases, the dividing point shifts further toward the tip, and convection dominates for a larger region.
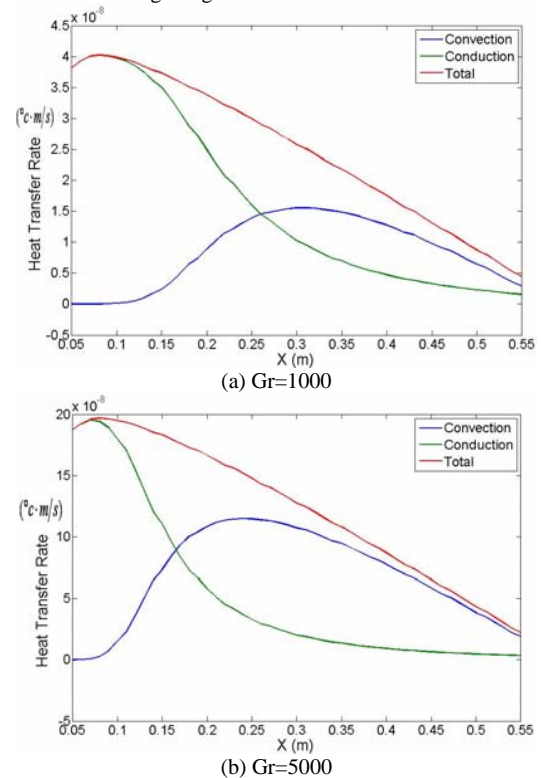

(a) Gr=1000

(b) Gr=5000

Figure 4 The horizontal heat transfer rate at the steady state averaged over the local water depth at different horizontal positions for Grashof numbers in the medium range.

A series of numerical simulations have been conducted with medium Grashof numbers of Gr = 500, 800, 1000, 3000, and 5000, respectively. The calculated dividing point is plotted against the Grashof number in Figure 5. The result shown in figure 5 confirms the above observation with regard to the shift of the dividing points toward the tip as the Grashof number increases.
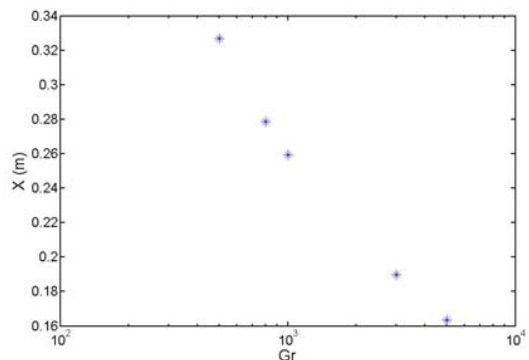

Figure 5 Horizontal dividing point at different Grashof number, Gr=500, 800, 1000, 3000, 5000

The local Rayleigh number for a fluid layer heated from below is defined as [2]:

$$Ra_T = \frac{g\beta T_b \delta^3}{\upsilon k} \qquad (13)$$

Substituting (8) and (9) into (13), we have

$$Ra_T \sim \Pr Gr \left(\frac{t}{h^2/k}\right)^2 e^{-A\eta x} \qquad (14)$$

Instabilities set in when the local Rayleigh number is larger than the critical Rayleigh number Ra_c [2]. Although the local Rayleigh number is a function of time, there is a limit for the growth of the local Rayleigh number with time. When the flow reaches its steady state at t_c, the thermal boundary layer ceases to grow. At this time t_c, T_b and δ_T both reach their maximum values, and thus Ra_T also reaches its maximum value $Ra_T(t_c)$. If this value is still less than the critical value Ra_c, the flow will become steady without any instability. However, if the Grashof number is sufficiently large so that $Ra_T(t_c) > Ra_c$, instability sets in after time t_B ($t_B < t_c$) when Ra_T becomes larger than Ra_c.

(a) Gr=10^5
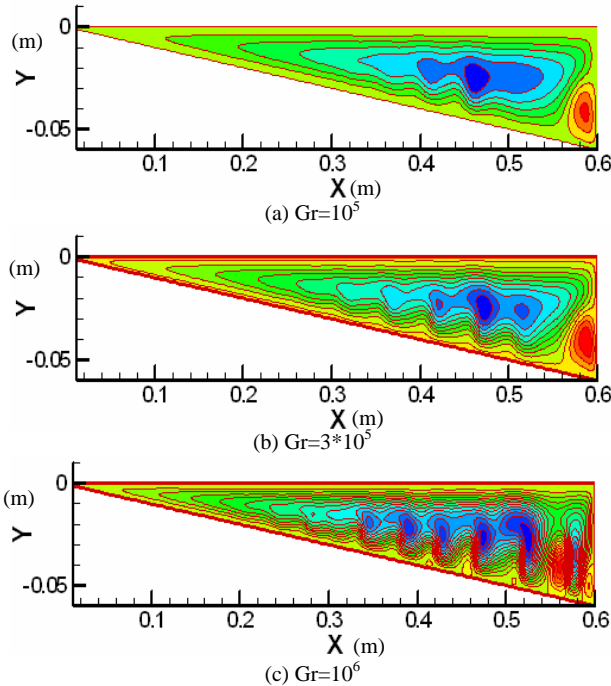

(b) Gr=$3*10^5$

(c) Gr=10^6

Figure 6 Streamlines at the steady state for high Grashof numbers.

Figure 6 shows the streamlines of the steady state flows for three different Grashof numbers which are sufficiently high to generate instability: Gr = 10^5, 3×10^5, and 10^6. The wavy structure above the bottom surface of the wedge is a result of flow instability. It is clear that the instability occurs over a certain range of the flow domain near the far end. The range and intensity of the instability increase with the Grashof number. This feature was confirmed quantitatively in Figure 7.

Figure 7 shows the calculated horizontal heat transfer rate averaged over the local depth at the steady state. Assuming the horizontal position where conduction equals convection is $x=a$, and the position where the wavy structure starts is $x=b$, there are three distinct regions dominated by different modes of heat transfer: for $x<a$, conduction dominates over convection in the
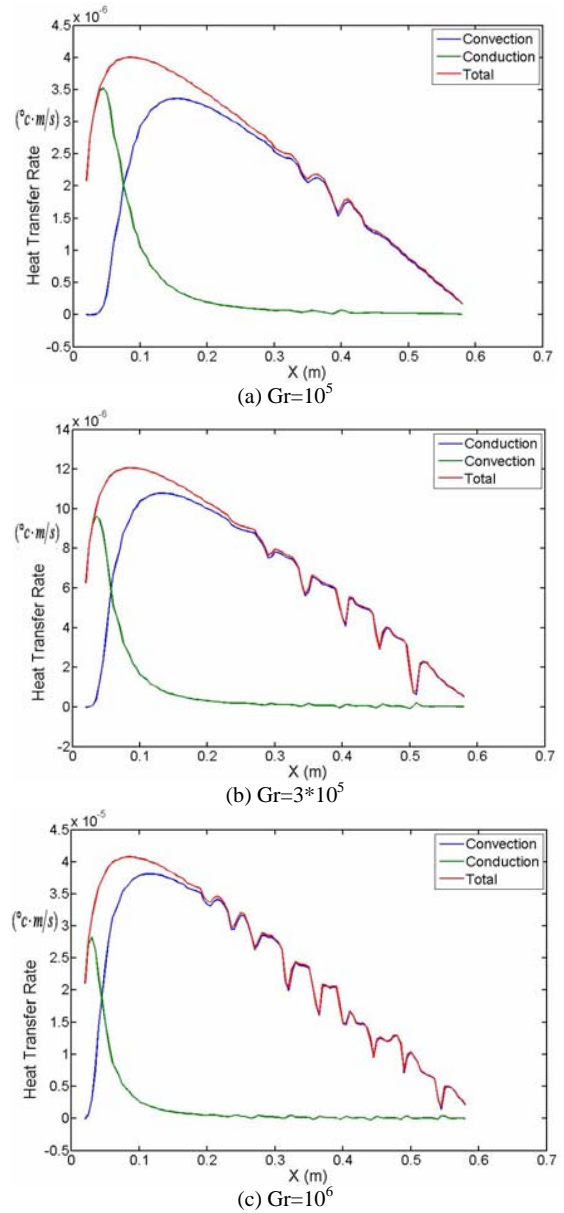

(a) Gr=10^5

(b) Gr=$3*10^5$

(c) Gr=10^6

Figure 7 The horizontal heat transfer rate at the steady state averaged over the local water depth at different horizontal positions for high Grashof numbers.

horizontal heat transfer; for $a<x<b$, stable convection dominates; and for $x>b$, flow instability occurs and unstable convection dominates. The unstable convection corresponds to the wavy structure in the streamlines in Figure 6. In the near tip region ($x<a$), the thermal boundary layer grows over the entire water depth before convection becomes significant, resulting in an indistinct thermal boundary layer. In the region $a<x<b$, after the time t_c, convection balances conduction, and the thermal boundary layer ceases to grow and remains distinct. In this region, the local Rayleigh number has also reached its maximum value at time t_c. Since the maximum local Rayleigh number in this region is less than the critical Rayleigh number Ra_c, the boundary layer is stable. In the region $x>b$, since the critical time t_B required for the local Rayleigh number to grow higher than Ra_c is shorter than the steady-state time t_c required

for convection to balance conduction, the thermal boundary layer becomes unstable. As the Grashof number increases, the region with flow instability expands toward the tip, and the intensity of the instability increases with the Grashof number.

Summary

The results of present numerical simulations have revealed the variations of the dominant mode of heat transfer and the flow status with the horizontal position along the wedge. This series of simulations has shed light on various flow scenarios at different Rayleigh numbers. For small Rayleigh numbers, conduction dominates the horizontal heat transfer over the whole domain with no distinct thermal boundary layer at the steady state. For medium Rayleigh numbers, a dividing point, where conduction heat transfer is equal to convection heat transfer at the steady state, splits the flow domain into two distinct regions: conduction dominates in the region close to the tip where isotherms are approximately vertical; convection is the dominant mode of the horizontal heat transfer in the deeper region, and the thermal boundary layer is distinct. The region dominated by convection at the steady state expands with the Rayleigh number. For high Rayleigh numbers, there are two dividing points: one between conduction and stable convection regions, and the other between stable and unstable convection regions. In the near tip region, conduction dominates, and the thermal boundary layer is indistinct. In the middle region, convection dominates and the thermal boundary layer is distinct and stable. In the deep region, the thermal boundary layer is unstable, and heat transfer is dominated by unstable convection.

Reference:
[1] Adams E. E. & Wells S. A., Field Measurements on Side Arms of Lake Anna, *J. Hyd. Eng*, **110**, 1984, 773-793.
[2] Drazin, P. G. & Reid, W. H., Hydrodynamic Stability. Cambridge University Press, 1981.
[3] Farrow, D. E. & Patterson, J. C. On the Response of a Reservoir Sidearm to Diurnal Heating and Cooling. *J. Fluid Mech.* **246**, 1993, 143-161.
[4] Farrow, D. E. & Patterson, J. C. The Daytime Circulation and Temperature Structure in a Reservoir Sidearm, *Intl J. Heat Mass Transfer* **37**, 1994, 1957-1968.
[5] Kirk, J. T. O., Optical Limnology-A Manifesto. in *Limnology in Australia*, editors, P. De Deckker & W. D. Williams, CSIRO Australia and Dr W. Junk., 1986, 33-62.
[6] Lei, C & Patterson, J. C., Unsteady Natural Convection in a Triangular Enclosure Induced by Absorption of Radiation, *J. Fluid Mech,* **460**, 2002, 181-209.
[7] Monismith S. G., Imberger J. & Morison M. L., Convective Motions in the Sidearm of a Small Reservoir, *Limnol. Oceanogr*, **35**, 1990, 1676-1702.